Journal of Ceramic Processing Research. Vol. 21, No. 6, pp. 705~711 (2020)
(Received 23 July 2020, Received in revised form 7 September 2020, Accepted 2 October 2020)
https://doi.org/10.36410/jcpr.2020.21.6.705

J O U R N A L O F
Ceramic Processing Research

Ce^{3+} and Eu^{2+} doped Sialon dual phosphor ceramic plates for white light emitting diodes

Bhupendra Joshi* and Gobinda Gyawali*
Department of Fusion Science and Technology, Sun Moon University, Chungnam 31460, Republic of Korea

Recent studies on transparent polycrystalline phosphor ceramic plates (PCPs) show its potential application in high brightness laser lighting. Herein, we explore the luminescence properties of Ce^{3+} cation in transparent Sialon phosphor ceramic plate. The green luminescence was observed in Ce^{3+} doped Sialon PCP as excited by the 390 nm wavelength. Also, the redshift of emissions was observed when the excitation wavelength was modulated from UV to blue light. The matrix phases and lattice parameters of Sialon PCPs were analyzed by XRD. The co-doping of Y^{3+} cations resulted a composite α/β-Sialon phase while doping with Gd^{3+} produced a higher α-Sialon phase. Higher transparency was observed with Gd^{3+} co-doped sample with greenish-yellow luminescence under blue light excitation. The optical properties of Gd-α-Sialon: Eu^{2+} was also investigated. Moreover, a broadband white light was obtained after placing Gd-α-Sialon: Eu^{2+} on the top of the Gd^{3+}/Ce^{3+} doped Sialon as a dual plate under blue LED excitation.

Keywords: Sialon, Transparency, Phosphor ceramic plate, Luminescence.

Introduction

The improvement in the stability of conventional phosphor-converted white light-emitting diode (pc-wLED) can be achieved by introducing stable phosphor with high thermal conductivity [1]. The plate type phosphors such as phosphors in glasses (PiGs) and glass-ceramics were studied as remote phosphors. However, the poor thermal and mechanical properties, as well as poor homogeneity of phosphor in the glass matrix, made it less suitable for high brightness lighting [2, 3]. Moreover, the low refractive index of glass causes poor light extraction [4]. Also, single-crystal phosphor plates were reported, but they are difficult to be commercialized in terms of cost-effectiveness. Therefore, polycrystalline transparent phosphor ceramic plates (PCPs) having similar physical properties to the single crystals are studied as future phosphors for high luminance and longevity solid-state lighting (SSL) [4].

Polycrystalline ceramics, such as garnet systems, have been studied as a PCP for wLED. However, the thermal conductivity of these oxide ceramics is low to be applied in high power light-emitting diode (LED) or laser diode (LD) for lightings [5]. The silicon aluminum oxynitride (Sialon) which is a solid solution of Si_3N_4 ceramics and exhibits excellent mechanical and thermal properties as well as chemical stability [6]. In general, the two common phases of Sialon ceramics were studied as phosphors, i.e., α-Sialon phase and β-Sialon phase, which are isostructure to α-Si_3N_4 phase and β-Si_3N_4, respectively [7]. The partial substitution of Si and N with Al and O, respectively in β-Si_3N_4, gives β-Sialon structure having a hexagonal crystal structure with a space group of $P6_3$. To compensate the charge within the α-Si_3N_4 structure, the metal cations are introduced in interstitial sites to form a stable α-Sialon phase after partial substitution of Si and N with Al and O, respectively having a formula of $M_x^{v+}Si_{12-m-n}Al_{m+n}O_nN_{16-n}$, where x=m/v and M is one of the metal cations (Li^+, Mg^{++}, Ca^{++} and most of the lanthanide ions (Ln^{3+})) [8]. The α-Sialon has a trigonal crystal structure with a space group of P31c. The powder form of Europium doped Calcium alpha Silicon Aluminum Oxynitride (Ca-α-Sialon: Eu^{2+}) phosphor was reported a decade ago, and later on, more studies were carried out on Sialon phosphors matching the properties required for warm white light [9]. As mentioned above, the powder phosphors either in resin or glass have issues with homogeneous distribution within the matrix. Recently, the transparent/translucent polycrystalline Sialon ceramics were studied as phosphor materials for down-conversion and upconversion PCPs [10-13]. The transparent/translucent Sialon PCPs can be applied in high power lighting and lighting in extreme conditions due to their outstanding physical and thermal properties.

In this article, Ce^{3+} was studied as an alternative to Eu^{2+} in the Sialon PCPs. The Ce^{3+} has fast luminescence decays than Eu^{2+}, which makes Ce^{3+} a more suitable activator than Eu^{2+} for high brightness solid-state lighting [14]. Also, Ce^{3+} has a broadband emission similar to Eu^{2+} due to the $4f^05d^1 \rightarrow 4f^1$ transition. The

*Corresponding author:
Tel : +82-41-530-2882
Fax: +82-41-530-2840
E-mail: joshibhupen@sunmoon.ac.kr / ggobinda@sunmoon.ac.kr

cerium element is more abundant in nature than the europium and lowers the production cost of phosphor with cerium in Sialon ceramics. Herein, we tried to investigate the luminescence properties of Ce^{3+} cation in transparent/translucent Sialon PCP. In previous reports, α-Sialon: Ce^{3+} shows blue to cyan emission with near UV excitation, which is not suitable to be used in blue LED chips. In contrast to previous reports [14-16], we observe intense greenish-yellow emission with Gd^{3+} co-doping along with Ce^{3+} under blue light excitation in Sialon PCP, which is discussed in this study.

Experimental

The two different compositions were made based on the formula, $M_x^{\nu+}Si_{12-m-n}Al_{m+n}O_nN_{16-n}$, where x=m/ν and M is one of the metal cations. The samples SC (Y^{3+} co-doped with Ce^{3+}) and SGC (Gd^{3+} co-doped with Ce^{3+}) were fabricated with compositions of $Y_{0.24}Ce_{0.05}Si_{10.65}Al_{1.35}O_{0.45}N_{15.55}$ (m = 2n = 0.9) and $Gd_{0.29}Ce_{0.08}Si_{9.8}Al_{2.2}O_{1.1}N_{14.9}$ (m = n = 1.1), respectively. For comparison, we prepared Gd^{3+} stabilized α-Sialon: Eu^{2+} (SE) with composition of $Gd_{0.28}Eu_{0.09}Si_{9.8}Al_{2.2}O_{1.1}N_{14.9}$ (m = n = 1.1). The powders used were α-Si_3N_4 (SN-E10, UBE Co., Japan), Al_2O_3 (High purity chemicals Co. Ltd., Japan), AlN (Grade F, Tokuyama Corp., Japan), CeO_2 (High Purity Chemicals Co. Ltd., Japan), Gd_2O_3 (High Purity Chemicals Co. Ltd., Japan), Y_2O_3 (High Purity Chemicals Co. Ltd., Japan) and Eu_2O_3 (High Purity Chemicals Co. Ltd., Japan). For the homogeneous mixing of powders, the powders were mixed in absolute ethanol in a polyethylene bottle with high purity silicon nitride balls, and wet ball milled for 24 h. Then, the mixed wet powder was dried in a rotary evaporator and then kept in an oven at 80 ºC for 12 h. The dried powder was then dry ball milled with high purity silicon nitride balls for 12 h. After dry ball milling, the mixed powder was sieved through 150 μm aperture sieve.

For hot press sintering, 15 g of mixed powder was packed into the graphite mold with an inner diameter of 50 mm. The inner parts of the graphite mold, disc, and graphite papers were coated with boron nitride to inhibit the carbon diffusion from the graphite into samples. The samples were hot press sintered at 1,850 ºC with 30 MPa of uniaxial pressure in the N_2 environment, and holding time was 1 h. The samples were ground to 0.1 mm thickness, and both sides were mirror polished to measure the transmittance and luminescence properties. The phases were analyzed by XRD. The relative amount of α-Sialon phase and β-Sialon phase in sintered ceramics was investigated based on the following equation [17];

$$X_\alpha = \frac{I_\alpha(102)+I_\alpha(210)}{K[I_\beta(101)+I_\beta(210)]+I_\alpha(102)+I_\alpha(210)} \quad (1)$$

where, X_α is the weight fraction of the α-Sialon phase, K is the constant referred to the relative intensity ratio and dependent on the chosen reflection (K=0.647).

The microstructure of the fracture surfaces was studied by the scanning electron microscope (SEM, SNE-3000, SEC, Co. Ltd., Korea). The light transmittance and luminescence were measured by UV/Vis/NIR Jasco 570 spectroscopy and Andor spectrophotometer, respectively. A commercial 455 nm blue LED chip (Model: T56-3BLZ-05, IST, Korea) was coupled with Sialon PCPs to obtain spectral power distribution curves (Ocean Optics USB2000 spectrophotometer).

Results and Discussion

The XRD patterns in Fig. 1 show that the sample SC is a composite of α and β phases in almost similar ratio, whereas the sample SGC has a dominant α-Sialon phase. In addition, the AlN polytypoid (JCPDS-42-161) and unidentified peak around 50º (2θdegree) were also observed in the XRD pattern of SC. The AlN polytypoid (12H) is commonly found in the sintered Sialon ceramics [18]. Also, in samples SGC and SE, a very small peak of the 12H phase was observed. The observed unidentified peak in SC may be of intermediate nitride/oxynitride phase [19, 20]. The two samples were prepared with different stabilizing cations, i.e., Y^{3+} and Gd^{3+} for samples SC and SGC, respectively. The Si was used as an internal standard to investigate the lattice parameters. The lattice parameters of SGC were increased as compared to SC (Table 1). The increase in cell parameters of SGC can be related to the insertion of Gd^{3+} cation, which has a larger cationic size as compared to Y^{3+}. Similarly, the sample SE also shows a dominant α-Sialon phase with an increase in cell parameters. The weight fraction of α and β phases were obtained from the equation (1) [17] and shown in Table 1. This expression is usually applied in silicon nitride based ceramics where more than two phases exist in sintered ceramics [17, 21, 22]. The grain morphologies of the fracture surface are shown in Fig. 2. The α-Sialon grains are considered to have small polyhedral grains, whereas β-Sialon grains are elongated and large. The large β-Sialon grains were observed in SC (Fig. 2(c)), which is also supported by the XRD, where the β-Sialon phase was observed. For SGC (Fig. 2a), the small grains were observed as compared to SC. The EDS analysis (Fig. 2(b and d)) shows that the sample consists of the desired composition, and wt% of different elements are tabulated in the inset table in Fig. 2(b), and Fig. 2(d) for sample SGC and SC, respectively. The low amount of additives was used in SC to make the higher nitrogen containing system as compared to SGC. When the composition is m = 2n, the additive alumina is excluded [6]. The system m = n = 1.1 is known to have better optical properties, where a higher amount of additives with alumina can be added with

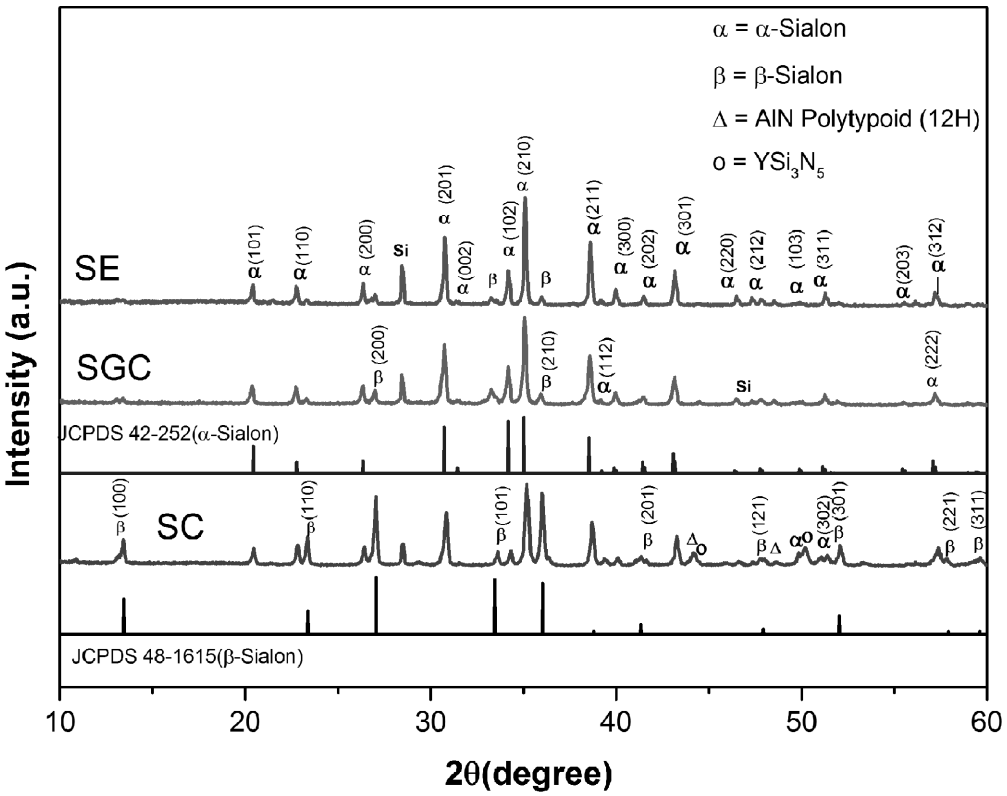

Fig. 1. XRD patterns of different samples with standard samples for comparison.

Table 1. Phase composition and cell parameters of Sialon ceramics.

Samples	Sialon phase (vol.%)		α-Sialon		β -Sialon	
	α-Sialon	β-Sialon	a (Å)	c (Å)	a (Å)	c (Å)
SC	65	35	7.78	5.65	7.61	2.89
SGC	88	12	7.81	5.69		
SE	92	8	7.81	5.68		

more stabilizer cations [11]. However, the system uses a higher amount of oxides and contains more oxygen in the grains. Also, an increase in liquid phase in SGC allows more rare earth cations to diffuse into the grains, and a higher α-Sialon phase was obtained. As seen in Table 1, the sample SE had a higher α-Sialon phase than SGC. The increase in α-phase in SE can be corroborated to the lower viscosity of Eu_2O_3 than other rare earth oxides at higher temperatures which forms more liquid phase and promotes the diffusion of rare earth cations in Sialon lattice to form α-Sialon phase [10].

The secondary phase inclusion in the ceramics degrades the transparency due to the mismatch of refractive indices between the grains and secondary phase. The polycrystalline ceramics are not free from defects such as grain boundaries, pores, dislocations, secondary phase, etc. Therefore, the optical properties degrade with increasing the thickness of the polycrystalline ceramics. In Fig. 3, the transmittance spectra are shown for different samples. The SGC had higher transparency than the SC sample. The higher α-Sialon phase was observed for SGC (Table 1), and this phase is considered to have a higher optical bandgap than β-Sialon give rise to higher transparency [23]. The composite phase in SC degrades the transparency of the material. Moreover, higher transparency was observed for the sample SE, which consisted of the highest α-Sialon phase as compared to other samples. The Sialon ceramics are fabricated by the addition of sintering additives, and therefore, it is difficult to eliminate the secondary phases that cause poor transparency in visible wavelength of light. Also, the colors of the SC, SGC, and SE samples correspond to grey, yellowish-green, and yellowish-orange, respectively, as shown in the inset in Fig. 3.

Fig. 4(a) shows the excitation spectra of SC and SGC. The sample SC has the highest excitation peak at 330 nm and covered the broad range from UV to violet region. Whereas the sample SGC shows different excitation spectra than SC, and the peak was redshifted to a bluish region. The main excitation peak was observed around 400 nm and extended to the blue spectrum. The excitation spectrum of SE is shown in Fig. 4(b). The excitation spectrum is broader than SC and SGC samples, which covers more in the blue region. Fig. 5(a) shows the luminescence spectra of sample SC from blue to green emissions. Different excitation wavelengths from 310-420 nm were used. The emissions

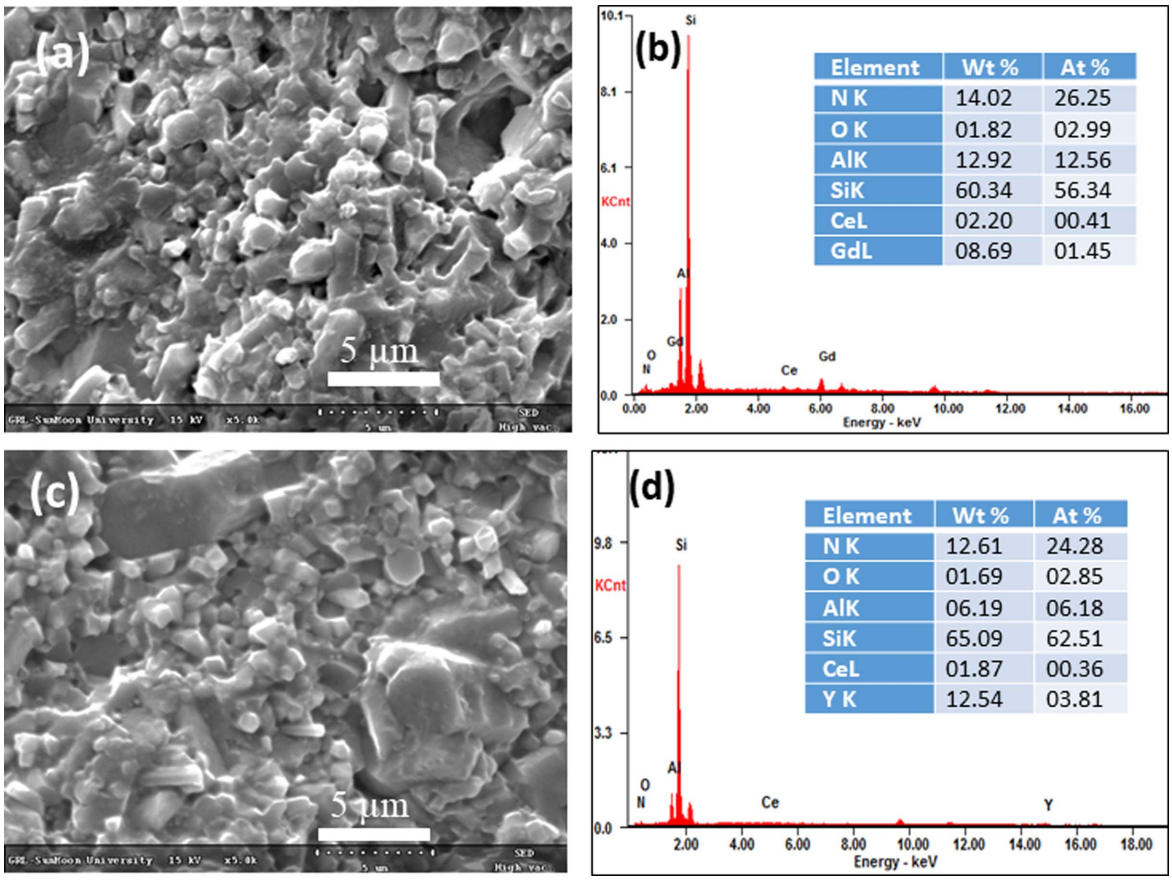

Fig. 2. SEM images of fracture surfaces of samples showing the grain morphology; (a) SGC and (c) SC. EDS analysis of fracture surfaces; (b) SGC and (d) SC.

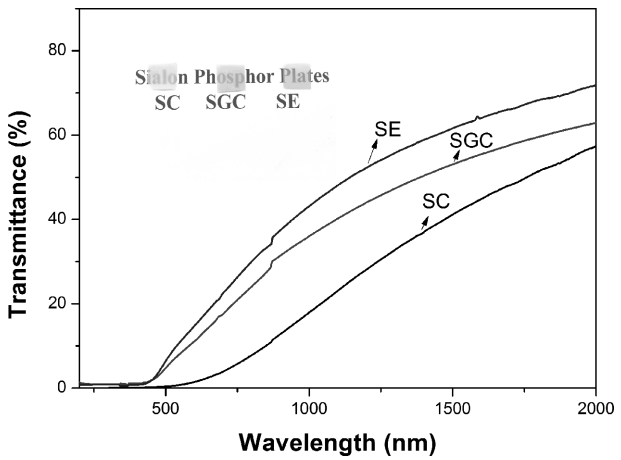

Fig. 3. Transmittance spectra of polished Sialon ceramics, and inset is the optical image of 0.1 mm thickness samples.

were redshifted with increasing the excitation wavelength. The excited samples had broadband emission from 420 to 600 nm wavelengths with bluish-green emission. The highest emission was achieved when excited by 330 nm wavelength (Fig. 5(a)), which is congruent with the excitation spectrum of SC (Fig. 4(a)). The quenching of the emission occurred when excited beyond 330 nm. Around 600 nm, small emissions were observed with lower wavelength excitation, which may be due to the impurity phase that exists in SC. The emission might be from the yttrium silicon nitride/ oxynitride phase with cerium ion. There are reports on luminescence from $Y_{6+x/3}Si_{11-y}Al_yN_{20+x-y}O_{1-x+y}$: Ce^{3+} and Ce^{3+}-doped $Y_3Si_5N_9O$ having orange emission [19, 20].

The redshift of emissions was also observed for SGC as increasing the excitation wavelengths (Fig. 5(b)). Greenish-yellow luminescence was observed in SGC. The highest emission was observed when excited with 390 nm wavelength and is congruent with the excitation spectrum of SGC (Fig. 4(a)). Comparing the emissions of SC and SGC excited at 390 nm, the emission wavelength was redshifted with a difference of 20 nm. Moreover, the SGC was further excited with blue light (450-470 nm), and the emissions were observed at 555 nm (Fig. 5(c)), whereas the SC was not excited with these wavelengths. The sample SE has shown emission in the orange region, and the redshift was not observed on increasing the excitation wavelength (Fig. 5(d)). The broad emission of the sample SE suggests that the emission was due to the 4f-5d transition. The precursor, Eu_2O_3, used had (III) oxidation state, which was reduced to (II) oxidation state during the fabrication of Sialon phosphor [10]. The sharp emissions of f-f

transition for Eu^{3+} were not observed in the emission spectra (Fig. 5(d)) also confirmed the reduction of Eu^{3+} to Eu^{2+}. The broad excitation band corresponds to $4f^7 \rightarrow 4f^6 5d$ transition of Eu^{2+} (Fig. 4(b)). The broad emission centered at 590 nm as excited by blue wavelengths (440-490) was due to the allowed $4f^6 5d \rightarrow 4f^7$ transition of Eu^{2+} [11].

The addition of Gd^{3+} ion in YAG: Ce reported by Chen et al. [24] also exhibited a redshift in emission. There are also reports on Ce^{3+} doped Sialon phosphor powders with different emissions, but the redshifting of emissions with increasing the excitation wavelength was not reported. The co-doping of different stabilizing cations such as Y^{3+} and Ca^{2+} along with Ce^{3+} gives emissions in blue and green regions, respectively, as reported by Krevel et al. [16]. As observed from the inset in Fig. 3, the color of the SGC is yellowish-green, which is originated from the absorption by Gd^{3+} and Ce^{3+} in the blue region. Also, the SGC had higher α-phase than SC, and thus higher Ce^{3+} should be

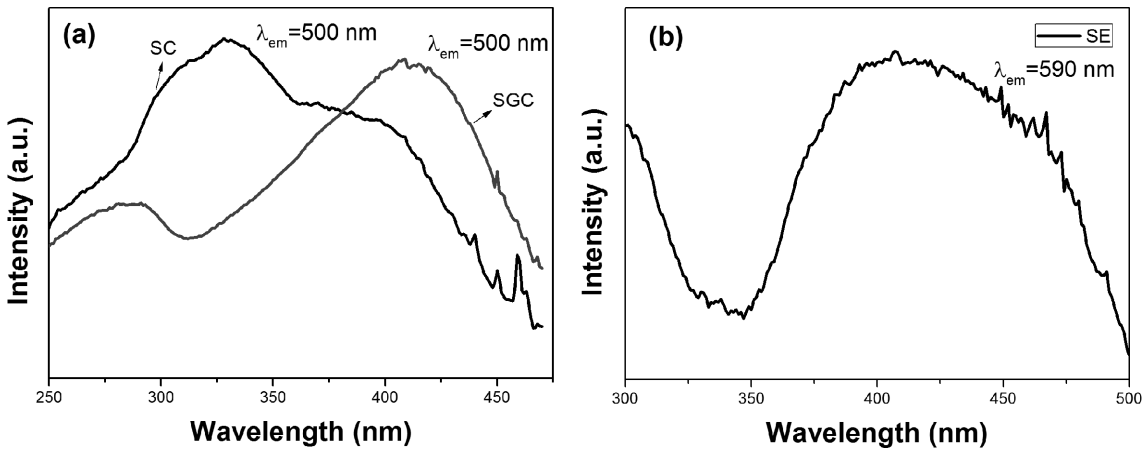

Fig. 4. (a) Excitation spectra of samples SC and SGC. (b) Excitation spectrum of SE.

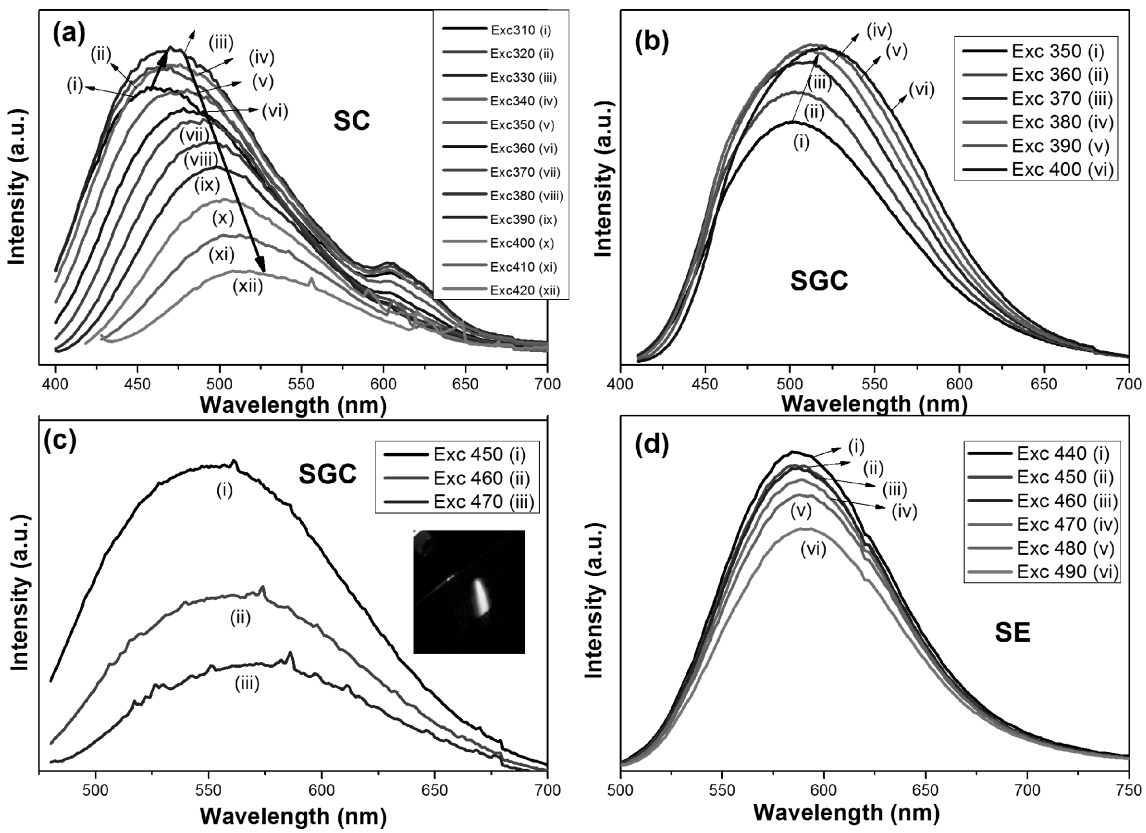

Fig. 5. (a) Emission spectra with different excitation wavelengths from 310-420 nm for sample SC, (b) emission spectra of SGC with different excitation wavelengths (350-400 nm), (c) emission spectra of SGC excited from 450-470 nm and inset image showing greenish-yellow emission excited by blue light, and (d) the emission spectra of SE excited from 440 -490 nm.

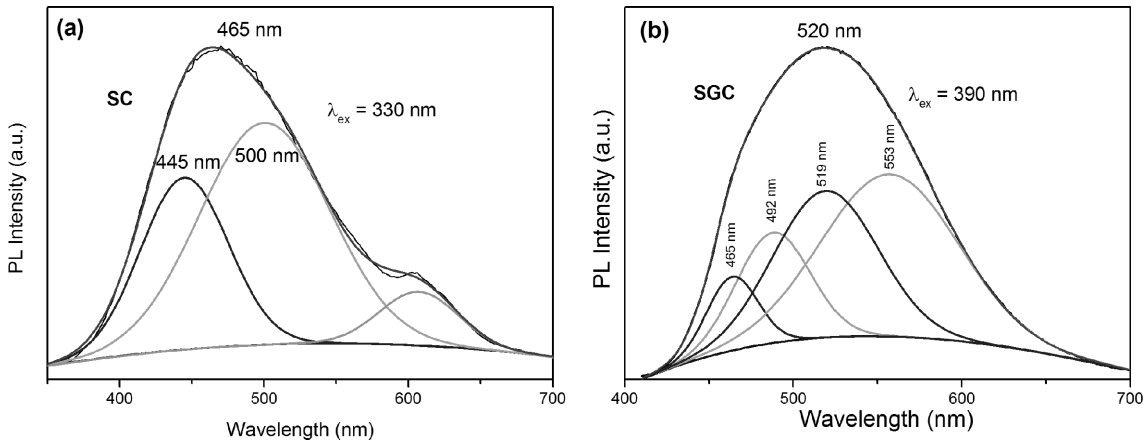

Fig. 6. Deconvoluted emission spectra of samples excited by 390 nm wavelength; (a) SC and (b) SGC.

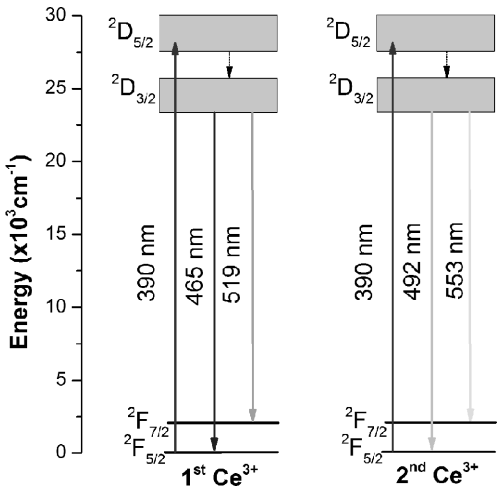

Fig. 7. Schematic energy levels diagram of Ce^{3+} in SGC.

incorporated along with Gd^{3+} in the α-Sialon matrix.

The ground state electronic configuration of Ce^{3+} was taken into account to explain the redshift of emissions while increasing the excitation wavelength. The electronic configuration $4f^1$ has two $^2F_{7/2}$ and $^2F_{5/2}$ manifolds separated by ~2,000 cm^{-1} showing two emissions within the broad emission band [14]. The Gaussian deconvolution of sample SC (Fig. 6(a)) excited at the lower wavelength (330 nm) shows two main emissions at 445 nm and 500 nm, which have an energy difference of 2,000 cm^{-1}. The other deconvoluted peak at 603 may be from the impurity phase in SC. Similarly, the SGC emission excited at 390 nm was deconvoluted (Fig. 6(b)) and four emissions at 465 nm, 492 nm, 519 nm, and 553 nm were observed. In the SGC sample, the amount of Ce^{3+} was higher than the SC sample. Therefore, interstitial doping of Ce^{3+} in the α-Sialon phase is also higher. The Ce atom is bonded to nitrogen atoms and oxygen atoms. The number of nitrogen and oxygen bonded to Ce atom in α-Sialon changes the crystal field splitting strength. The four fitted peaks were also reported by Wang et al. [25]. The energy difference of 465 nm and 519 nm, as well as 492 nm and 553 nm, were around 2000 cm^{-1}. Both samples had an energy difference of approximately ~2,000 cm^{-1}, which matches the energy difference of $^2F_{7/2}$ and $^2F_{5/2}$ states of Ce^{3+}. Thus the shift in emission can be attributed to the $^2F_{7/2}$ and $^2F_{5/2}$ ground states. The energy level diagram of Ce^{3+} in SGC is shown in Fig. 7. In blue light excitations, the yellowish-green emission becomes more prominent, as seen in Fig. 5(c). Therefore, the 4f ground state of Ce^{3+} is split into two $^2F_{7/2}$ and $^2F_{5/2}$ states, and bluish-green emission arose from the $^2D_{3/2} \rightarrow {}^2F_{5/2}$ transition, whereas the yellowish-green emission was originated from $^2D_{3/2} \rightarrow {}^2F_{7/2}$ transition.

The excitation with higher energy UV light had $^2F_{5/2}$

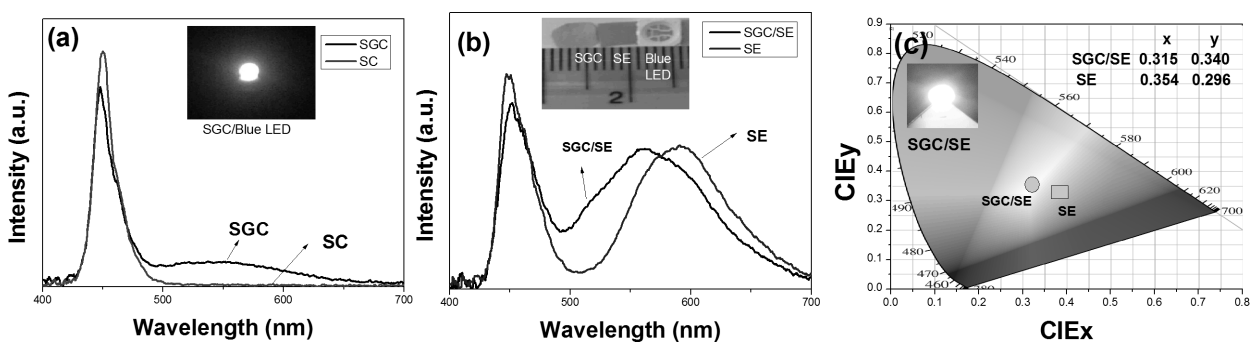

Fig. 8. (a) Spectral distribution curves for samples SC and SGC as excited by blue LED (455 nm), (b) Blue LED excited luminescence from dual plates, and (c) CIE chromaticity diagram showing the color co-ordinates for dual plates with CIE co-ordinate values.

$\rightarrow {}^2D_{5/2}$ transition, whereas the low energy blue light with ${}^2F_{5/2} \rightarrow {}^2D_{3/2}$ transition. The prominent bluish-green emission with UV excitation was observed from the radiative ${}^2D_{3/2} \rightarrow {}^2F_{5/2}$ transition. Similarly, the yellowish-green emission was seen with blue light irradiation due to the ${}^2D_{3/2} \rightarrow {}^2F_{7/2}$ transition. The redshift of emission in sample SGC as compared to SC can be corroborated to the large cationic size of Gd^{3+} ion as compared to Y^{3+}. The large cationic size of Gd^{3+} ion shortened the Ce-N/O distance and increased the crystal field splitting [26].

The PCPs were placed on the blue LED with 455 nm wavelength. The spectral distribution curves are shown in Fig. 8(a). The sample SGC shows greenish-yellow emission while there is no emission with sample SC. Greenish-yellow emission of SGC can be combined with orange emission that can cover a wide visible spectrum to get white light. To obtain a wide emission, the SGC PCP was combined with transparent SE PCP. A wide spectrum from blue to red centered at 560 nm (yellow) was obtained for dual plates with sample SGC/SE, as observed in Fig. 8(b). The luminous efficacies of SGC/SE and SE had 50 lm/W and 46 lm/W, respectively. As seen from the CIE co-ordinates in Fig. 8(c), the dual plates (SGC/SE) is near to the white region. The color co-ordinate temperatures were measured as 4,189 K and 6,292 K for SE plate and SE/SGC dual plate, respectively.

Conclusion

In conclusion, the greenish-yellow emitting transparent Sialon phosphor ceramic plates were fabricated by the hot press sintering method. The α/β-composite Sialon and α-Sialon PCPs with Ce^{3+} doping show green emission, and the latter sample shows greenish-yellow emission with blue excitation. The sample having Gd^{3+} ion as a stabilizer had higher transparency, and emission shifted to the yellow region as compared to the Y^{3+} stabilized sample. The blue light excited broad emission with greenish-yellow emission was achieved with Gd^{3+} co-doping with Ce^{3+} ion. Also, the optical properties of Eu^{3+} doped Sialon were investigated. Moreover, the dual plates show a wider spectrum near to the white region of the CIE chromaticity diagram.

References

1. S. Pimputkar, J.S. Speck, S.P. DenBaars, and S. Nakamura, Nat. Photonics 3 (2009) 180-182.
2. H. Segawa, S. Ogata, N. Hirosaki, S. Inoue, T. Shimizu, M. Tansho, S. Ohki, and K. Deguchi, Opt. Mater. 33 (2010) 170-175.
3. X. Zhang, J. Yu, J. Wang, B. Lei, Y. Liu, Y. Cho, R.J. Xie, H. W. Zhang, Y. Li, Z. Tian, Y. Li, and Q. Su, ACS Photonics 4 (2017) 986-995.
4. S. Li, L. Wang, N. Hirosaki, and R.J. Xie, Laser Photonics Rev. 12 (2018) 1800173.
5. S. Li, Q. Zhu, D. Tang, X. Liu, G. Ouyang, L. Cao, N. Hirosaki, T. Nishimura, Z. Huang, and R.J. Xie, J. Mater. Chem. C 4 (2016) 8648-8654.
6. B. Joshi, G. Gyawali, H. Wang, T. Sekino, and S. W. Lee, J. Alloy. Compd. 557 (2013) 112-119.
7. Y.J. Park, J.M. Kim, and J.W. Lee, J. Ceram. Process. Res. 16 (2015) 578-583.
8. B. Joshi, G. Gyawali, and S.W. Lee, Lett. Mater. 10 (2020) 158-163.
9. H.L. Li, N. Hirosaki, R.J. Xie, T. Suehiro, and M. Mitomo, Sci. Technol. Adv. Mater. 8 (2007) 601-606.
10. B. Joshi, Y.K. Kshetri, G. Gyawali, and S.W. Lee, J. Alloy. Compd. 631 (2015) 38-45.
11. B. Joshi, J. S. Hoon, Y.K. Kshetri, G. Gyawali, and S.W. Lee, Ceram. Inter. 44 (2018) 23116-23124.
12. B. Joshi, and S.W. Lee, J. Rare Earths 33 (2015) 1142-1147.
13. B. Joshi, Y.K. Kshetri, G. Gyawali, and S.W. Lee, J. Ceram. Process. Res. 17 (2016) 197-201.
14. H.L. Li, G.H. Zhou, R.J. Xie, N. Hirosaki, X.J. Wang, and Z. Sun, J. Solid. State Chem. 184 (2011) 1036-1042.
15. L. Gan, F.F. Xu, X.H. Zeng, Z.S. Li, Z.Y. Mao, P. Lu, Y.C. Zhu, X.J. Liu, and L.L. Zhang, Nanoscale 7 (2015) 11393-11400.
16. J.W.H. van Krevel, J.W.T. van Rutten, H. Mandal, H.T. Hintzen, and R. Metselaar, J. Solid. State Chem. 165 (2002) 19-24.
17. D.J. Devlin, and K.E. Amin, Powder Diffr. 5 (1990), 121-124.
18. W. He, Q. Liu, and H. Zhong, Mater. Sci. Eng., A 528 (2011) 8359-8364.
19. W. B. Park, S. P. Singh, M. Pyo, and K.S. Sohn, J. Mater. Chem. 21 (2011) 5780-5785.
20. Q.Q. Zhu, L. Wang, N. Hirosaki, L.Y. Hao, X. Xu, and R.J. Xie, Chem. Mater. 28 (2016) 4829-4839.
21. C.P. Gazzara, and D.R. Messier, Amer. Ceram. Soc. Bull. 56 (1977) 777-780.
22. Z. Mencik, M. Short, and C. Peters, Adv. X-Ray Anal. 23 (1979) 375-379.
23. B. Joshi, B. Li, Y.K. Kshetri, H. Wang, and S.W. Lee, Ceram. Int. 40 (2014) 13041-13047.
24. J. Chen, Z. Deng, Z. Liu, Y. Lin, D. Chen, B. Fei, C. Wang, F. Wang, Q. Hu, and Y. Cao, Opt. Express 23 (2015) A292-A298.
25. Q. Wang, Z. Ci, G. Zhu, M. Que, S. Xin, Y. Wen, and Y. Wang, ECS J. Solid State Sci. Technol. 1 (2012) R92-R97.
26. Y. Du, C.Y. Shao, Y.J. Dong, Q.H. Yang, and W. Hua, Chinese Phys. B 24 (2015) 117801.